NJC

PAPER

View Article Online
View Journal | View Issue

Cite this: *New J. Chem.*, 2014, **38**, 4434

A coumarin-based sensitive and selective fluorescent sensor for copper(II) ions†

Jiun-Ting Yeh, Wei-Chieh Chen, Shi-Rong Liu and Shu-Pao Wu*

Received (in Montpellier, France) 30th April 2014,
Accepted 24th June 2014

DOI: 10.1039/c4nj00695j

www.rsc.org/njc

A new coumarin-derived fluorescent probe (**1**) exhibited significant fluorescence quenching in the presence of Cu^{2+} ions. Other metal ions, *e.g.* Ag^{+}, Ca^{2+}, Cd^{2+}, Co^{2+}, Fe^{2+}, Fe^{3+}, Hg^{2+}, K^{+}, Mg^{2+}, Mn^{2+}, Ni^{2+}, Pb^{2+}, and Zn^{2+}, produced only minor changes in the fluorescence of chemosensor **1**. The binding ratio of the chemosensor–Cu^{2+} complexes was found to be 2 : 1, according to Job plot experiments. The association constant (K_a) for Cu^{2+} binding with chemosensor **1** was found to be 9.56×10^9 M^{-2}. The maximum fluorescence quenching caused by Cu^{2+} binding with chemosensor **1** occurred over a pH range of 5–9. Moreover, fluorescence microscopy experiments showed that chemosensor **1** could be used as a fluorescent probe for detecting Cu^{2+} in living cells.

1 Introduction

The development of highly selective chemosensors for the recognition of environmentally and biologically important metal ions, such as Cu^{2+}, Cd^{2+}, Fe^{3+}, Hg^{2+}, Pb^{2+}, and Zn^{2+}, has been a key issue in research.[1–5] Copper, after iron and zinc, is the third most abundant essential transition metal ion in the human body, and plays vital roles in several natural processes.[6] Many proteins use copper ions as their catalytic center. However, copper ions also catalyze the formation of reactive oxygen species (ROS) that can harm lipids, nucleic acids, and proteins. Several research studies have linked the cellular toxicity of copper ions to serious diseases such as Alzheimer's disease,[7] Indian childhood cirrhosis (ICC),[8] prion disease,[9] and Menkes and Wilson diseases.[10] Due to its widespread application, the copper ion is also a significant metal pollutant. The limit of copper in drinking water as set by the US Environmental Protection Agency (EPA) is 1.3 ppm (~20 μM).

The determination of copper ions in various samples has been an important topic in the area of environmental protection and food safety. Several methods have been applied for the detection of copper ions, including atomic absorption spectrometry,[11] inductively coupled plasma mass spectroscopy (ICPMS),[12] inductively coupled plasma-atomic emission spectrometry (ICP-AES),[13] and voltammetry.[14] Most of these methods require expensive instruments and are not suitable for direct assays. Recently, more attention has been focused on the development of fluorescent chemosensors for the detection of Cu^{2+} ions.[15–28]

In this study, a new coumarin derivative **1** containing a phenol hydrazone moiety was designed for metal ion detection. Two components make up chemosensor **1**; a coumarin moiety as a reporter, and a phenol hydrazone moiety as a metal ion chelator (Scheme 1). Binding metal ions to chemosensor **1** causes fluorescence quenching of coumarin. The metal ions Ag^{+}, Ca^{2+}, Cd^{2+}, Co^{2+}, Fe^{2+}, Fe^{3+}, Hg^{2+}, K^{+}, Mg^{2+}, Mn^{2+}, Ni^{2+}, Pb^{2+}, and Zn^{2+} were tested for metal ion binding with chemosensor **1**. Cu^{2+} was the only ion that caused significant fluorescence quenching upon binding with chemosensor **1**.

2 Results and discussion

2.1 Synthesis of chemosensor 1

Chemosensor **1** was synthesized by the reaction of phenol hydrazone and 7-diethylaminocoumarin-3-aldehyde to form an imine bond between phenol hydrazone and coumarin (Scheme 1). Chemosensor **1** is light yellow and has an absorption band centered at 467 nm. Chemosensor **1** exhibits a green emission band centered at 537 nm with a quantum yield of Φ = 11.5%.

2.2 Cation-sensing properties

The sensing ability of chemosensor **1** was tested by mixing it with the metal ions Ag^{+}, Ca^{2+}, Cd^{2+}, Co^{2+}, Cu^{2+}, Fe^{2+}, Hg^{2+}, K^{+}, Mg^{2+}, Mn^{2+}, Ni^{2+}, Pb^{2+}, and Zn^{2+}. Cu^{2+} was the only metal ion causing a visible color change from light yellow to red and green fluorescence quenching (Fig. 1). During Cu^{2+} titration with chemosensor **1**, the absorbance at 487 nm decreased, and a new band centered at 440 nm was formed (Fig. 2). The color change from light yellow to red revealed this 47 nm blue shift.

To further evaluate the selectivity of chemosensor **1** towards various metal ions, the fluorescence spectra of chemosensor **1**

Department of Applied Chemistry, National Chiao Tung University, Hsinchu, Taiwan 300, Republic of China. E-mail: spwu@mail.nctu.edu.tw; Fax: +886-3-5723764; Tel: +886-3-5712121 ext. 56506

† Electronic supplementary information (ESI) available: ^{1}H and ^{13}C NMR spectra of chemosensor **1**, ESI mass spectra of the Cu^{2+}–$\mathbf{1}_2$ complexes and the calibration curve of **1**–Cu^{2+} (10 μM) in a methanol–water solution. See DOI: 10.1039/c4nj00695j

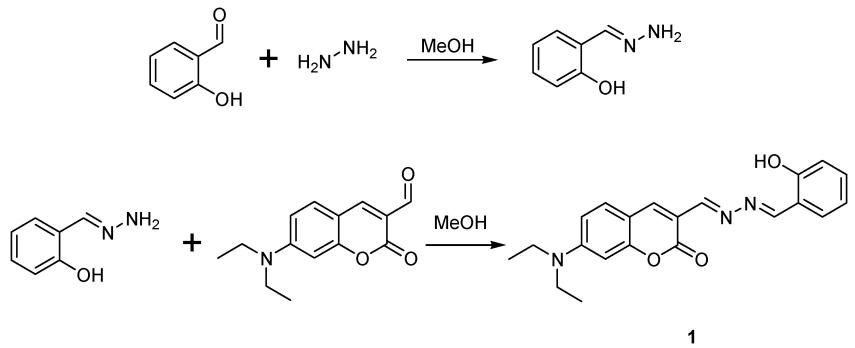

Scheme 1 Synthesis of chemosensor **1**.

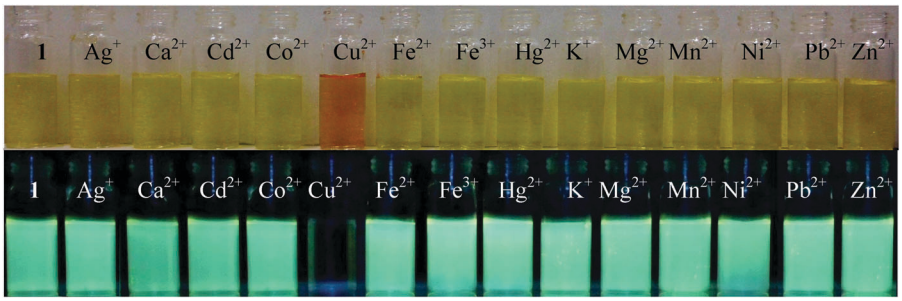

Fig. 1 Color (top) and fluorescence (bottom) changes in **1** upon the addition of various metal ions in a methanol–water (v/v = 1 : 1, 10 mM HEPES, pH 7.0) solution.

were taken in the presence of several metal ions. However, Cu^{2+} was the only metal ion that caused significant fluorescence quenching (Fig. 1). During Cu^{2+} titration with chemosensor **1**, the intensity of the 537 nm emission band decreased (Fig. 2). After the addition of greater than one equivalent of Cu^{2+}, the emission intensity reached a minimum. These observations suggest that Cu^{2+} is the only metal ion that readily binds with chemosensor **1**, causing significant fluorescence quenching and permitting highly selective detection of Cu^{2+}.

To study the influence of other metal ions on Cu^{2+} binding with chemosensor **1**, we performed competitive experiments with other metal ions (20 μM) in the presence of Cu^{2+} (20 μM) (Fig. 3). The fluorescence quenching caused by the Cu^{2+} solution with most other metal ions was similar to that caused by Cu^{2+} alone. This indicates that the other metal ions do not interfere significantly with the binding of chemosensor **1** to Cu^{2+}.

In order to understand the binding stoichiometry of chemosensor **1**–Cu^{2+} complexes, Job plot experiments were carried out. In Fig. 4, the emission intensity at 537 nm is plotted against the molar fraction of chemosensor **1** at a constant total concentration (20 μM). The minimum emission intensity was reached when the molar fraction was 0.67. These results indicate a 2 : 1 ratio for **1**–Cu^{2+} complexes, in which one Cu^{2+} binds with two chemosensor **1** molecules. The formation of a Cu^{2+}–$\mathbf{1}_2$ complex was also confirmed by ESI-MS, in which the peak at m/z = 788.7 indicates a 1 : 2 stoichiometry for the $[Cu + \mathbf{1}_2\text{–}H]^+$ complex (see Fig. S4 in the ESI†). The association constant, K_a, was evaluated graphically by plotting $\alpha^2/(1 - \alpha)$ *vs.* $1/[Cu^{2+}]$, where α is defined as $[F - F_0]/[F_1 - F_0]$ (Fig. 5). The data were linearly fitted, and the K_a value was determined from the slope and the intercept of the line. The association constant (K_a) for Cu^{2+} binding in chemosensor **1** was found to be $9.56 \times 10^9\ M^{-2}$. The limit of detection for chemosensor **1** as a fluorescent sensor for Cu^{2+} detection was determined from a plot of fluorescence intensity as a function of Cu^{2+} concentration (see Fig. S5 in the ESI†). It was found that chemosensor **1** has a limit of detection of 0.27 μM, which allows for the detection of Cu^{2+} ions in the micromolar concentration range.

To gain a clearer understanding of the structure of the Cu^{2+}–$\mathbf{1}_2$ complexes, ^1H NMR spectroscopy (Fig. 6) was employed. Cu^{2+} is a paramagnetic ion which affects the NMR resonance frequency of protons that are close to the Cu^{2+} binding site. The ^1H NMR spectra of chemosensor **1**, recorded with increasing amounts of Cu^{2+}, show that the proton signal (H_f, OH) at δ = 11.2 ppm almost completely disappears upon the addition of Cu^{2+} (Fig. 6). The proton signal (H_e, imine) at δ = 8.65 ppm became broader as Cu^{2+} was added, indicating that Cu^{2+} binds to the nitrogen atom at the imine bond. Other peaks remained unchanged. These observations indicate that Cu^{2+} binds to chemosensor **1** through one imine nitrogen atom and one hydroxyl oxygen atom.

To elucidate the structure of the Cu^{2+}–$\mathbf{1}_2$ complexes, we employed density functional theory (DFT) calculations using the Gaussian 09 software package. Chemosensor **1** and Cu^{2+}–$\mathbf{1}_2$ complexes were subjected to energy optimization using B3LYP/6-31G and B3LYP/LANL2DZ, respectively. The global minima structure for the Cu^{2+}–$\mathbf{1}_2$ complex is shown in Fig. 7. The distances of Cu^{2+} from the two oxygen atoms were 1.90 Å and 1.90 Å, and those from the two nitrogen atoms were 2.01 Å and 2.02 Å.

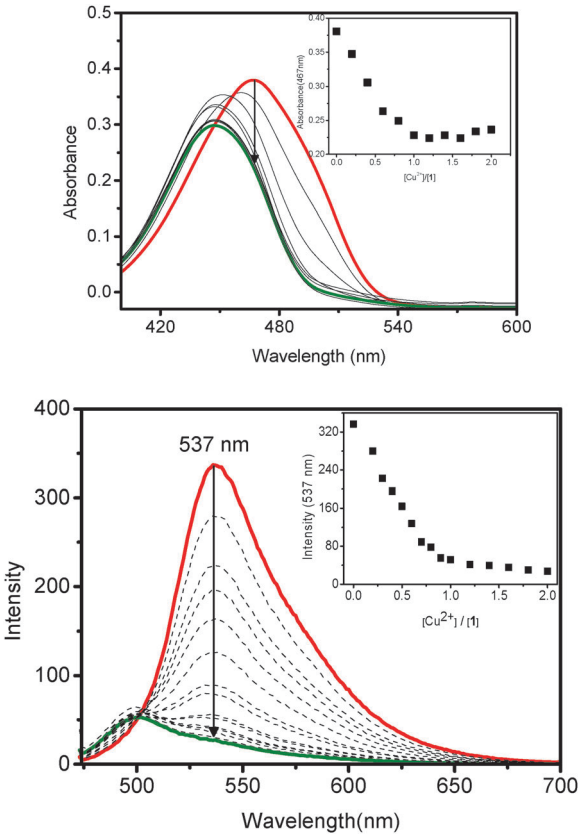

Fig. 2 Absorption (top) and emission spectra (bottom) of **1** (10 μM) in methanol–water (v/v = 1 : 1, 10 mM HEPES, pH 7.0) solution upon the addition of 0–2.0 μM of Cu^{2+}. The excitation wavelength was 467 nm.

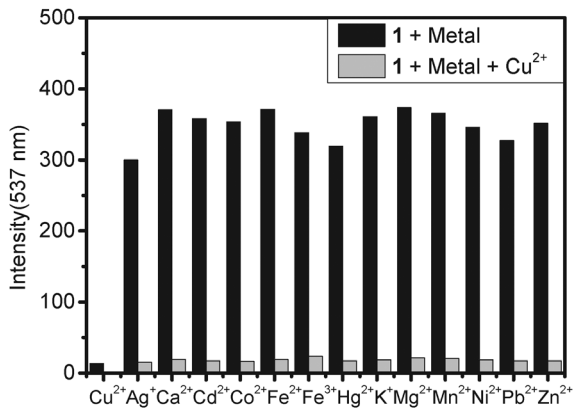

Fig. 3 Fluorescence response of **1** (10 μM) to Cu^{2+} (20 μM) or 20 μM of other metal ions (the black bar) and to the mixture of other metal ions (20 μM) with 20 μM of Cu^{2+} (the gray bar) in methanol–water (v/v = 1 : 1, 10 mM HEPES, pH 7.0) solutions.

We performed pH titration of chemosensor **1** to determine a suitable pH range for Cu^{2+} sensing. In Fig. 8, the emission intensities of metal-free chemosensor **1** at most pH values are high. When the pH is higher than 9, the emission intensities decrease slightly due to deprotonation of the hydroxy group in chemosensor **1**. After mixing chemosensor **1** with Cu^{2+}, the emission intensity at 537 nm suddenly decreased in the pH

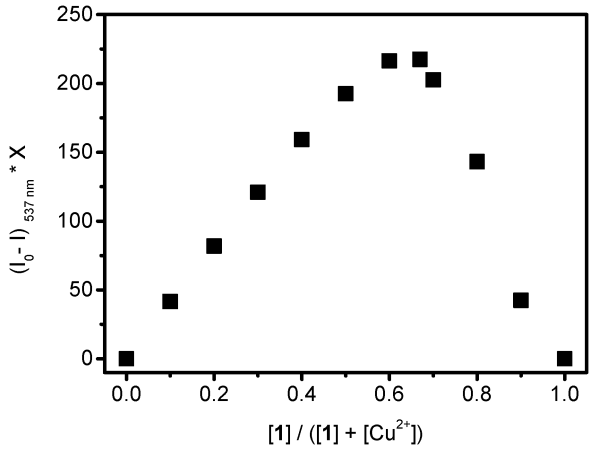

Fig. 4 Job plot of **1**–Cu^{2+} complexes, where the emission intensity at 537 nm is plotted against mole fraction of **1**, at a constant total concentration of 2.0 × 10^{-5} M in methanol–water (v/v = 1 : 1, 10 mM HEPES, pH 7.0) solutions.

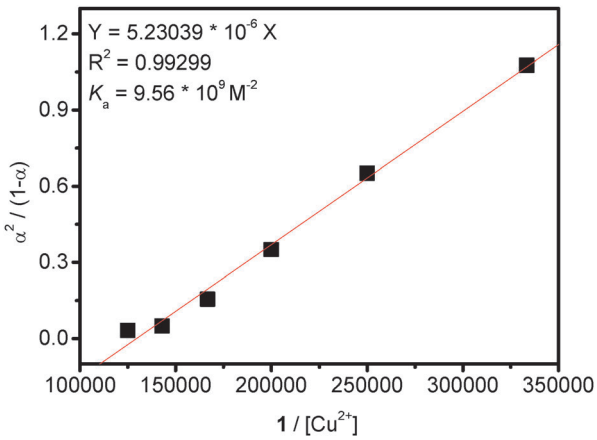

Fig. 5 The plot of chemosensor **1** with Cu^{2+} in methanol/water (v/v = 1 : 1, 10 mM HEPES, pH 7.0) solution. The excitation wavelength was 467 nm and the observed wavelength was 537 nm.

range of 5.0 to 9.0. When the pH was lower than 5, the emission intensity at 537 nm increased slightly, compared to that at pH 7.0. This is due to protonation on the Schiff base, preventing the formation of the Cu^{2+}–$\mathbf{1}_2$ complex.

For a chemosensor to be extensively used in the detection of specific targets, reversibility is an important issue. To explore whether the binding process of chemosensor **1** with Cu^{2+} is reversible, an excess amount of CN^- was added into a solution of chemosensor **1** with Cu^{2+}. In Fig. 9, the emission peak at 537 nm increases significantly after addition of CN^-. When Cu^{2+} was added to the system, the fluorescence of **1** was again quenched. This observation indicates the reversibility of the binding of chemosensor **1** with Cu^{2+}.

2.3 Living cell imaging

Chemosensor **1** was also tested for living cell imaging. First, HeLa cells incubated with **1** displayed a strong fluorescence image (Fig. 10). The overlapping of the fluorescence and bright

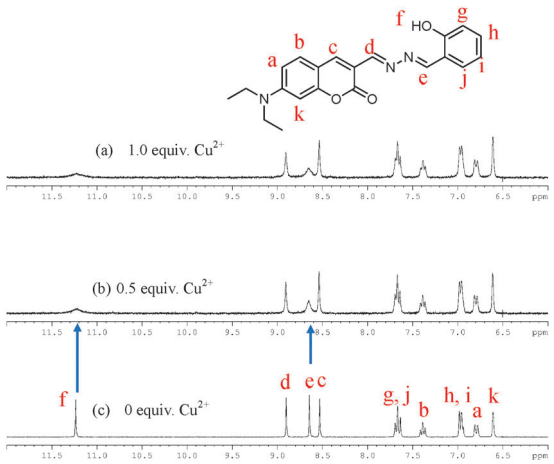

Fig. 6 ^{1}H NMR spectra of chemosensor **1** (10 mM) in the presence of different amount of Cu^{2+} in DMSO-d_6.

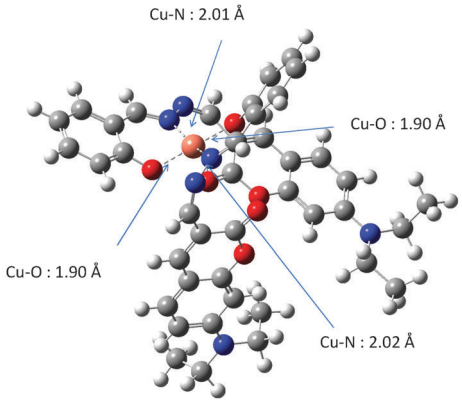

Fig. 7 DFT-optimized structures of Cu^{2+}–$\mathbf{1}_2$ complexes calculated using the B3LYP/LanL2DZ method. (Red atom, O; blue atom, N; orange atom, Cu).

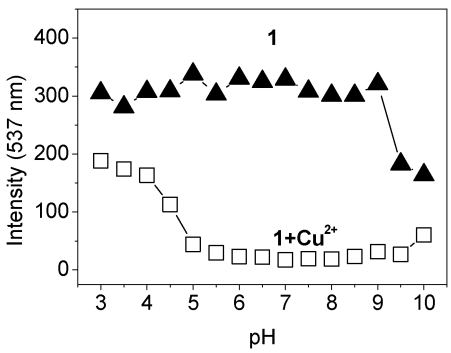

Fig. 8 Fluorescence response of free chemosensor **1** (10 μM) (▲) and after addition of Cu^{2+} (20 μM) (□) in methanol–water (v/v = 1 : 1, 10 mM buffer, pH 3–4: PBS; pH 4.5–6: MES; pH 6.5–8.5: HEPES; pH 9–10: Tris-HCl) solution as a function of different pH values. The excitation wavelength was 467 nm.

field images reveals that the fluorescence signals are localized in the intracellular area, indicating good cell membrane permeability of chemosensor **1**. After further treatment with Cu^{2+}, the

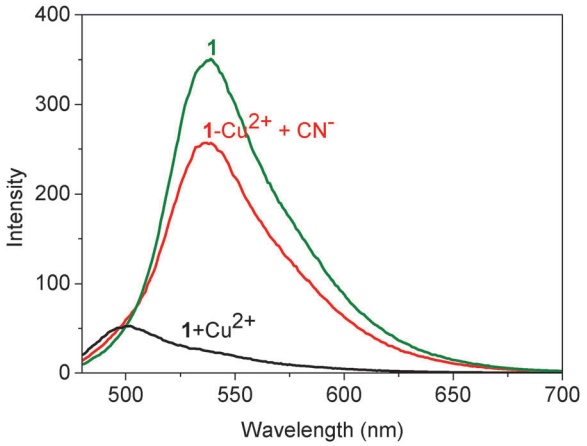

Fig. 9 Reversibility of the interaction between **1** and Cu^{2+} by the introduction of CN^- to the system.

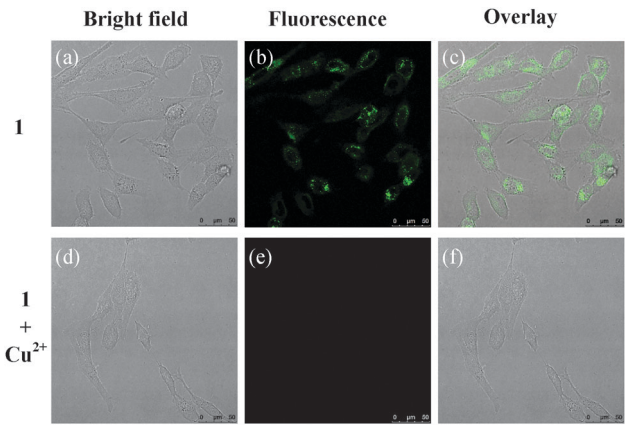

Fig. 10 Fluorescence images of HeLa cells treated with **1** and $Cu(BF_4)_2$. (left) Bright field image; (middle) fluorescence image; and (right) merged image.

fluorescence vanished. These observations demonstrate effective binding of chemosensor **1** with Cu^{2+}.

3 Conclusions

In this study, a coumarin-based fluorescent chemosensor, chemosensor **1**, was developed for Cu^{2+} detection. Significant fluorescence quenching was observed with chemosensor **1** in the presence of Cu^{2+} ions, while other metal ions, *e.g.* Ag^+, Ca^{2+}, Cd^{2+}, Co^{2+}, Fe^{2+}, Hg^{2+}, K^+, Mg^{2+}, Mn^{2+}, Ni^{2+}, Pb^{2+}, and Zn^{2+} caused only minor changes in fluorescence intensity. The optimal pH range for Cu^{2+} detection by chemosensor **1** is from 5–9. This coumarin-based Cu^{2+} chemosensor serves as an effective and non-destructive probe for Cu^{2+} detection in living cells.

4 Experimental section

4.1 Materials and instrumentation

All solvents and reagents were obtained from commercial sources and used as received without further purification. UV/Vis spectra

were recorded on an Agilent 8453 UV/Vis spectrometer. NMR spectra were obtained on a Bruker DRX-300 NMR and Varian Unity Inova 500 NMR spectrometer. IR data were obtained on Bomem DA8.3 Fourier-transform infrared spectrometer. Fluorescence images were obtained on a Leica TCS SP5 X AOBS confocal fluorescence microscope.

4.2 Synthesis of chemosensors 1

2-(Hydrazonomethyl)phenol (136 mg, 1.00 mmol)[29] and 7-diethylaminocoumarin-3-aldehyde (245 mg, 1.00 mmol)[30] were dissolved in 10 mL of methanol, and stirred overnight at room temperature. A red precipitate was formed, and the crude product was filtered, thoroughly washed with methanol to give **1**. Yield: 254 mg (70%). Melting point: 196–197 °C; ^{1}H-NMR (300 MHz, DMSO-d_6): δ 11.23 (s, 1H), 8.90 (s, 1H), 8.65 (s, 1H), 8.54 (s, 1H), 7.67 (t, J = 7.5 Hz, 2H), 7.39 (t, J = 6.9 Hz, 1H), 6.96 (t, J = 8.1 Hz, 2H), 6.80 (dd, J = 9.0 Hz, J = 2.1 Hz, 1H), 6.64 (d, J = 1.8 Hz, 1H), 3.48 (q, J = 6.6 Hz, 4H), 1.15 (t, J = 6.6 Hz, 6H); ^{13}C-NMR (125 MHz, DMSO-d_6): δ 162.1, 160.4, 158.6, 157.2, 156.8, 152.1, 141.4, 132.9, 131.5, 131.0, 119.5, 118.3, 116.4, 111.1, 110.0, 108.0, 96.4, 44.3, 12.3; IR (KBr): 3417, 2974, 2933, 1709, 1620, 1576 cm^{-1}; MS(EI): m/z (%) = 363 (100), 348 (26.6), 346 (37.8), 243 (38.4), 229 (59.5), 173 (87.4); HRMS (EI): m/z, calcd for $C_{21}H_{21}N_3O_3$ (M^+): 363.1583; found: 363.1588.

4.3 Metal ion binding study by fluorescence spectroscopy

Chemosensor **1** (10 μM) was added with different metal ions (20 μM). All spectra were measured in 1.0 mL methanol–water solution (v/v = 1 : 1, 10 mM HEPES, pH 7.0). The light path length of the cuvette was 1.0 cm.

For pH dependence experiments, the buffers were: pH 3–4: PBS; pH 4.5–6: MES; pH 6.5–8.5: HEPES; pH 9–10: Tris-HCl. The binding stoichiometry of **1**–Cu^{2+} complexes was determined by Job plot experiments. The fluorescence intensity at 537 nm was plotted against molar fraction of **1** at a constant total concentration (20 μM) of **1** and Cu^{2+}. The fluorescence approached a minimum intensity when the molar fraction was 0.67. These results indicate that chemosensor **1** forms a 2 : 1 complex with Cu^{2+}. The stability constants K_a of 2 : 1 **1**–Cu^{2+} complexes were determined by the equation:[31]

$$\alpha^2/(1 - \alpha) = 1/(2K_aC_F[M]) \quad (1)$$

where C_F is the total concentration of chemosensor **1** in the system and α is defined as the ratio between the free chemosensor **1** and the total concentration of chemosensor **1**. The value "α" was obtained using eqn (2)

$$\alpha = [F - F_0]/[F_1 - F_0] \quad (2)$$

where F is the fluorescence intensity at 537 nm at any given Cu^{2+} concentration, F_1 is the fluorescence intensity at 537 nm in the absence of Cu^{2+}, F_0 is the maxima fluorescence intensity at 537 nm in the presence of Cu^{2+}. The association constant K_a was evaluated graphically by plotting $\alpha^2/(1 - \alpha)$ against $1/[Cu^{2+}]$. The plot $\alpha^2/(1 - \alpha)$ *vs.* $1/[Cu^{2+}]$ is shown in Fig. 6. Data were linearly fitted according to eqn (1) and the K_a value was obtained from the slope of the line.

4.4 Cell imaging

The cell line HeLa was provided by the Food Industry Research and Development Institute (Taiwan). HeLa cells were cultured in Dulbecco's modified Eagle's medium (DMEM) supplemented with 10% fetal bovine serum (FBS) at 37 °C under an atmosphere of 5% CO_2. Cells were plated on 18 mm glass coverslips and allowed to adhere for 24 h.

Experiments to assess the Cu^{2+} uptake were performed in phosphate-buffered saline (PBS) with 20 μM $Cu(BF_4)_2$. The cells cultured in DMEM were treated with 20 mM solutions of chemosensor **1** (2 μL; final concentration: 20 μM) dissolved in DMSO and incubated at 37 °C for 30 min. The treated cells were washed with PBS (3 × 2 mL) to remove any remaining sensor. DMEM (2 mL) was added to the cell culture, which was then treated with a 10 mM solution of $Cu(BF_4)_2$ (2 μL; final concentration: 20 μM) dissolved in sterilized PBS (pH = 7.4). The samples were incubated at 37 °C for 30 min. The culture medium was removed, and the treated cells were washed with PBS (3 × 2 mL) before observation. Confocal fluorescence imaging of cells was performed using a Leica TCS SP5 X AOBS confocal fluorescence microscope (Germany), and a 63× oil-immersion objective lens was used. The cells were excited with a white light laser at 467 nm, and emission was collected at 517–557 nm.

4.5 Quantum chemical calculation

Quantum chemical calculations based on density functional theory (DFT) were carried out using a Gaussian 09 program. The ground-state structures of chemosensor **1** and the Cu^{2+}–$\mathbf{1}_2$ complexes were computed using the density functional theory (DFT) method with the hybrid-generalized gradient approximation (HGGA) functional B3LYP. The 6-31G basis set was assigned to nonmetal elements (C, H, N and O). For the Cu^{2+}–$\mathbf{1}_2$ complexes, the LANL2DZ basis set was used for Cu^{2+}, whereas the 6-31G basis set was used for other atoms.

Acknowledgements

We gratefully acknowledge the financial support of Ministry of Science and Technology (Taiwan) and National Chiao Tung University.

Notes and references

1 A. P. de Silva, H. Q. N. Gunaratne, T. Gunnlaugsson, A. J. M. Huxley, C. P. McCoy, J. T. Rademacher and T. E. Rice, *Chem. Rev.*, 1997, **97**, 1515–1566.
2 E. M. Nolan and S. J. Lippard, *Chem. Rev.*, 2008, **108**, 3443–3480.
3 N. Kaur and S. Kumar, *Tetrahedron*, 2011, **67**, 9233–9264.
4 M. Dutta and D. Das, *TrAC, Trends Anal. Chem.*, 2012, **32**, 113–132.
5 H. N. Kim, W. X. Ren, J. S. Kim and J. Yoon, *Chem. Soc. Rev.*, 2012, **41**, 3210–3244.
6 J. A. Cowan, *Inorganic Biochemistry: An Introduction*, Wiley-VCH, New York, 1997, pp. 133-134.

7 K. J. Barnham, C. L. Masters and A. I. Bush, *Nat. Rev. Drug Discovery*, 2004, **3**, 205–214.
8 S. H. Hahn, M. S. Tanner, D. M. Danke and W. A. Gahl, *Biochem. Mol. Med.*, 1995, **54**, 142–145.
9 D. R. Brown, *Brain Res. Bull.*, 2001, **55**, 165–173.
10 D. J. Waggoner, T. B. Bartnikas and J. D. Gitlin, *Neurobiol. Dis.*, 1999, **6**, 221–230.
11 A. P. S. Gonzales, M. A. Firmino, C. S. Nomura, F. R. P. Rocha, P. V. Oliveira and I. Gaubeur, *Anal. Chim. Acta*, 2009, **636**, 198–204.
12 J. S. Becker, A. Matusch, C. Depboylu, J. Dobrowolska and M. V. Zoriy, *Anal. Chem.*, 2007, **79**, 3208–3216.
13 Y. Liu, P. Liang and L. Guo, *Talanta*, 2005, **68**, 25–30.
14 P. Pathirathna, Y. Yang, K. Forzley, S. P. McElmurry and P. Hashemi, *Anal. Chem.*, 2012, **84**, 6298–6302.
15 H. S. Jung, P. S. Kwon, J. W. Lee, J. Kim, C. S. Hong, J. W. Kim, S. Yan, J. Y. Lee, J. W. Lee, T. Joo and S. Kim, *J. Am. Chem. Soc.*, 2009, **131**, 2008–2012.
16 S. Goswami, D. Sen and N. K. Das, *Org. Lett.*, 2010, **12**, 856–859.
17 D. Maity and T. Govindaraju, *Chem. – Eur. J.*, 2011, **17**, 1410–1414.
18 M. P. Algi, Z. Oztas and F. Algi, *Chem. Commun.*, 2012, **48**, 10219–10221.
19 J. Jo, H. Y. Lee, W. Liu, A. Olasz, C. Chen and D. Lee, *J. Am. Chem. Soc.*, 2012, **134**, 16000–16007.
20 Z. Liu, C. Zhang, X. Wang, W. He and Z. Guo, *Org. Lett.*, 2012, **14**, 4378–4381.
21 J. Fan, X. Liu, M. Hu, H. Zhu, F. Song and X. Peng, *Anal. Chim. Acta*, 2012, **735**, 107–113.
22 C. Kar, M. D. Adhikari, A. Ramesh and G. Das, *Inorg. Chem.*, 2013, **52**, 743–752.
23 H. Wang and S. Wu, *Sens. Actuators, B*, 2013, **181**, 743–748.
24 C. Chou, S. Liu and S. Wu, *Analyst*, 2013, **138**, 3264–3270.
25 X. Li, M. Yu, F. Yang, X. Liu, L. Wei and Z. Li, *New J. Chem.*, 2013, **37**, 2257–2260.
26 L. Zhang, Y. Zhang, M. Wei, Y. Yi, H. Li and S. Yao, *New J. Chem.*, 2013, **37**, 1252–1257.
27 H. Han, M. Wang and H. Wang, *New J. Chem.*, 2014, **38**, 914–917.
28 O. García-Beltrán, B. K. Cassels, N. Mena, M. T. Nuñez, O. Yañez and J. Caballero, *Tetrahedron Lett.*, 2014, **55**, 873–876.
29 S. H. Kim, S. Y. Gwon, S. M. Burkinshaw and Y. A. Son, *Dyes Pigm.*, 2010, **87**, 268–271.
30 J. Wu, W. Liu, X. Zhuang, F. Wang, P. Wang, S. Tao, X. Zhang, S. Wu and S. Lee, *Org. Lett.*, 2007, **9**, 33–36.
31 V. S. Jisha, A. J. Thomas and D. Ramaiah, *J. Org. Chem.*, 2009, **74**, 6667–6673.